OPEN ACCESS
ARTICLE

Silver Molybdate and Silver Tungstate Nanocomposites with Enhanced Photoluminescence

Invited Article

Yuri V. B. De Santana[1], José Ernane Cardoso Gomes[2], Leandro Matos[2], Guilherme Henrique Cruvinel[2], André Perrin[3], Christiane Perrin[3], Juan Andrès[4], José A. Varela[2] and Elson Longo[1,*]

1 CDMF/INCTMN-UNESP, Universidade Estadual Paulista, Araraquara, SP, Brazil
2 CDMF/INCTMN-UFSCar, Universidade Federal de São Carlos, São Carlos, SP, Brazil
3 Université de Rennes 1, Rennes cedex, France
4 Department of Experimental Sciences, Univ Jaume I, Spain
* Corresponding author Email: yurivbs@gmail.com

Received 09 May 2014; Accepted 21 Jul 2014

DOI: 10.5772/58923

© 2014 The Author(s). Licensee InTech. This is an open access article distributed under the terms of the Creative Commons Attribution License (http://creativecommons.org/licenses/by/3.0), which permits unrestricted use, distribution, and reproduction in any medium, provided the original work is properly cited.

Abstract Silver molybdate (Ag_2MoO_4) and silver tungstate (Ag_2WO_4) nanomaterials were prepared using two complementary methods, microwave assisted hydrothermal synthesis (MAH) (pH 7, 140 °C) and co-precipitation (pH 4, 70 °C), and were then used to prepare two core/shell composites, namely α-Ag_2WO_4/β-Ag_2MoO_4 (MAH, pH 4, 140 °C) and β-Ag_2MoO_4/β-Ag_2WO_4 (co-precipitation, pH 4, 70 °C). The shape and size of the microcrystals were observed by field emission scanning electron microscopy (FE-SEM), different morphologies such as balls and nanorods. These powders were characterized by X-ray powder diffraction and UV-vis (diffuse reflectance and photoluminescence). X-ray diffraction patterns showed that the Ag_2MoO_4 samples obtained by the two methods were single-phased and belonged to the β-Ag_2MoO_4 structure (spinel type). In contrast, the Ag_2WO_4 obtained in the two syntheses were structurally different: MAH exhibited the well-known tetrameric stable structure α-Ag_2WO_4, while co-precipitation afforded the metastable β-Ag_2WO_4 allotrope, coexisting with a weak amount of the α-phase. The optical gap of β-Ag_2WO_4 (3.3 eV) was evaluated for the first time. In contrast to β-Ag_2MoO_4/β-Ag_2WO_4, the α-Ag_2WO_4/β-Ag_2MoO_4 exhibited strongly-enhanced photoluminescence in the low-energy band (650 nm), tentatively explained by the creation of a large density of local defects (distortions) at the core-shell interface, due to the presence of two different types of MO_x polyhedra in the two structures.

Keywords Silver Molybdate, Silver Tungstate, Photoluminescence, Decorated System

1. Introduction

Tungstate ceramic materials are mixed oxides that can be used in numerous technological applications such as

humidity sensors [1], photocatalysts [2] electrochromic devices [3], Raman converters [4], scintillators [5], photoluminescent materials [6] and lasers [7-8]. α-Ag_2WO_4 can be considered an example of a high-dimensional and high-connected polyoxometalate-based hybrid compound [9-10] Pang et al. prepared superfine Ag_2WO_4 antibacterial powders with good antimicrobial durability [11] and using α-Ag_2WO_4 as a starting material, prepared an Ag/AgBr/WO_3.H_2O composite that exhibited good photocatalytic activity for the destruction of *Escherichia coli* bacteria under visible light and that was relatively stable under repeated use. [12]. Pan et al. [13] synthesized microstructured Ag_2WO_4 with a shuttle-like shape via a precipitation process with the assistance of Arabic gum. Aouadi et al. [14] studied the changes in the chemistry and crystal structure of $Ag_2Mo_2O_7$ and Ag_2WO_4 thin films and powders ranging between 25° and 600° C. In addition, they used *ab initio* molecular dynamics and different experimental techniques to explain the low coefficient of friction.

L.S. Cavalcante et al. observed and explained the photoluminescent behaviour of α-Ag_2WO_4 (i.e., $Ag_8W_4O_{16}$) microcrystals [15], in which Ag ions can display different AgOx corresponding to type-coordination and synergistic coordination modes in order to facilitate the formation of several clusters with low and high coordination numbers (x=2,4,6,7). The latter phase, which is the thermodynamically stable phase among several polymorphs, namely α- , β- , and γ- Ag_2WO_4 [16], has been found to be an interesting material, due to the growth of Ag filaments on its surface when it is exposed to electron beam irradiation [17]. Recently, controlled synthesis and the high photocatalytic activity of hierarchically porous metastable β-Ag_2WO_4 hollow nanospheres were reported by Wang et al. [18].

Consequently, silver tungstate Ag_2WO_4 has been receiving attention from the scientific community due to its vast scope for applicability. Its photoluminescent properties [19] and corresponding applications as a microbial agent [20], as well as its use as a novel ozone gas sensor [21], were investigated by our group.

Metal molybdates, another important family of inorganic materials, have also been intensively investigated because of their various properties, one of these being photoluminescence [22-24]. Several studies have been carried out to explore the properties and practical applications of silver molybdate Ag_2MoO_4, which exist in two forms, α-tetragonal [25] and β- cubic [26-27]. Silver molybdates have applications in areas such as high-temperature lubrication [28-29], ion-conducting glasses [30] and gas-sensing and surface enhanced Raman scattering techniques [31]. To date, flower-like [32] nanoparticles [33] and wire-like [34] have been obtained Tai et al. [35] reported the MAH synthesis of cube-like Ag-Ag_2MoO_4, which has visible-light photocatalytic activity. Low- dimensional silver molybdate-nanostructures have been obtained by Nagaraju et al., who reported the synthesis of nanorods/nanowires/multipods and the photoluminescence of microrods [36]. Lei et al. [37] reported on the room-temperature synthesis of Ag nanoparticles with decorated silver molybdate nanowires, using a solution-based chemical reaction method. Long et al. [31] published a facile hydrothermal technique for synthesizing Ag_2MoO_4 at relatively low temperatures (80 ºC and 20 ºC). Arora et al. [25] studied the behaviour of the cubic spinel phase of Ag_2MoO_4 at high pressure, as characterized by X-ray diffraction and Raman spectroscopy and very recently, a first-principles study of the pressure-induced phase transitions and electronic properties of Ag_2MoO_4 was conducted by our group [38]. Due to the potential applications of both Ag_2MoO_4 and Ag_2WO_4, our objective was to synthesize these two compounds using both a soft approach (direct precipitation at 70 °C) and a more energetic one, namely MAH. The latter has received much attention due to this technique offering significant advantages over conventional methods, including environmentally- friendly conditions, relatively low processing temperature and a short reaction time [39-40]. The same synthesis conditions have been used for the preparation of the Ag_2MO_4 (M = Mo, W) nanoparticles decorated with $Ag_2M'O_4$ (M' = W, Mo) in order to investigate new physical properties and in particular, the behaviour of photoluminescence (PL). Indeed, in previous studies, it has been shown that core/shell nanoparticles or decorated nanoparticles can exhibit strongly-enhanced luminescent properties compared to the PL properties of the two constituents building the nanoparticle [41-42]. It must be noted that such PL properties hold great technological and economic interest, which has stimulated the work presented here; photoluminescent materials are now being applied in various devices such as TVs, computers, calculators, LED screens and diodes, among others.

Three more sections complete this article. Next, we present the experimental details. In Section 3, the results are presented and discussed. A brief summary and the main conclusions will be offered in the final section.

2. Experimental Details

2.1 Synthesis of Ag_2WO_4, Ag_2MoO_4 and decorated nanoparticles

Two sets of samples were synthesized, with and without the use of MAH synthesis.

In the first set, silver tungstate was precipitated by mixing solutions of $Na_2WO_4.2H_2O$ and $AgNO_3$ (1 mmol and 2 mmol, respectively, in 50 ml of deionized water). The suspension was transferred in a PTFE autoclave and heated at 140 °C for 60 min with microwave assistance (2.45 GHz,

maximum power of 800 W). Then, the precipitate was separated by centrifugation, washed several times with deionized water and ethanol and dried at 70 °C for 24 hours. For reference, silver molybdate was prepared following the same procedure. In a second step, 0.2 g of silver tungstate was added to 50 mL of distilled H_2O and dispersed by ultrasonic agitation for 10 min. To this solution, 25 mL (1 mmol) of sodium molybdate and 25 mL (2 mmol) of silver nitrate were added under vigorous magnetic stirring. The pH of the solution was adjusted to 4 by the addition of nitric acid and the mixture was, as previously, heated at 140 °C for 60 min with microwave assistance. Separation and drying were applied as above. In the following, the two obtained compounds will be labelled as W-*htmw* and Mo-*htmw*, and the silver tungstate nanoparticles decorated by the silver molybdate as W/Mo-*htmw*.

For the second set, silver tungstate and silver molybdate were prepared by precipitation from sodium salts in aqueous solutions of pH 4 (nitric acid and distilled water). For silver tungstate, 1 mmol of $Na_2WO_4.2H_2O$ (99.5% purity, Sigma Aldrich) was dissolved in 50 ml of pH 4 solution (solution A). Separately, 2 mmol of $AgNO_3$ (99.8% purity, Sigma Aldrich) was dissolved in another 50 ml of the pH 4 aqueous solution (solution B). These two solutions were heated at 70 °C; then, solution B was added to solution A under vigorous magnetic stirring, after which the solution became dark grey. The mixture was kept at 70 °C for 10 min with stirring. Then, the precipitate was separated by centrifugation, washed several times with deionized water and ethanol, and dried at 70 °C for 24 hours. Silver molybdate was prepared following the same procedure using $Na_2MoO_4.2H_2O$ (99.5% purity, Sigma Aldrich). In the following, the obtained compounds will be labelled as *W-70* and *Mo-70*, respectively. To prepare silver molybdate nanoparticles decorated by the silver tungstate, 0.2 gr of sample *Mo-70* was added to 50 ml of the pH 4 solution and dispersed for 15 min by ultrasonic agitation. Then, 1 mmol of $Na_2WO_4.2H_2O$ and 2 mmol of $AgNO_3$ were dissolved separately in 25 ml of ph 4 solution (solutions 1, 2 and 3, respectively). The three solutions were heated at 70 °C and then solutions 2 and 3 were added to solution 1 sequentially and kept under agitation for 10 min. The silver tungstate nanoparticles decorated by the silver molybdate were prepared in a similar manner. The decorated samples obtained were labelled *Mo/W-70* and *W/Mo-70*.

2.2 Characterization of Ag2WO4, Ag_2MoO_4 and decorated nanoparticles

The Ag_2WO_4 and Ag_2MoO_4 microcrystals and the decorated nanoparticles were characterized by X-ray diffraction (XRD) patterns, using a D/Max-2000PC diffractometer Rigaku (Japan) with Cu Kα radiation (λ = 1.5406 Å) in the 2θ range from 10° to 70° in the normal routine and with a scanning velocity of 2°/min. The shapes and sizes of the Ag_2WO_4 and Ag_2MoO_4 microcrystals and decorated nanoparticles were observed with a FE-SEM model Inspect F50 (FEI Company, Hillsboro, OR), operated at 5 kV. UV-vis spectra were taken using a Varian spectrophotometer (model Cary 5G) in diffuse-reflectance mode. PL measurements were performed through a Monospec 27 monochromator (Thermal Jarrel Ash) coupled to a R446 photomultiplier (Hamamatsu Photonics, Japan). A krypton-ion laser (Coherent Innova 90K; λ = 350.7 nm) was used as the excitation source; its maximum output power was maintained at 500 mW. The laser beam was passed through an optical chopper and its maximum power on the sample was maintained at 40 mW. All PL measurements were performed at room temperature.

3. Results

3.1 X-ray diffraction

Figure 1 shows the powder XRD patterns of our silver molybdate (Mo-*htmw*) and silver tungstate (W-*htmw*) samples, as well as the synthesized composite (W/Mo-*htmw*) of the first set. It is obvious that the molybdate sample Mo-*htmw* was pure β-Ag_2MoO_4, as the pattern perfectly matched the JCPDS card no. 08-0473. This result supports previous reports and showed that this phase usually formed near pH 7 [32,40,43]. Similarly, the pattern of our silver tungstate W-*htmw* exactly matched the JCPDS card no. 34-0061, implying that the sample was perfectly monophased α-Ag_2WO_4, in good agreement with previous observations in neutral [15,44-46] or slightly alkaline [47] media. The profile of the W/Mo-*htmw* composite was essentially the superimposition of the patterns of the two components.

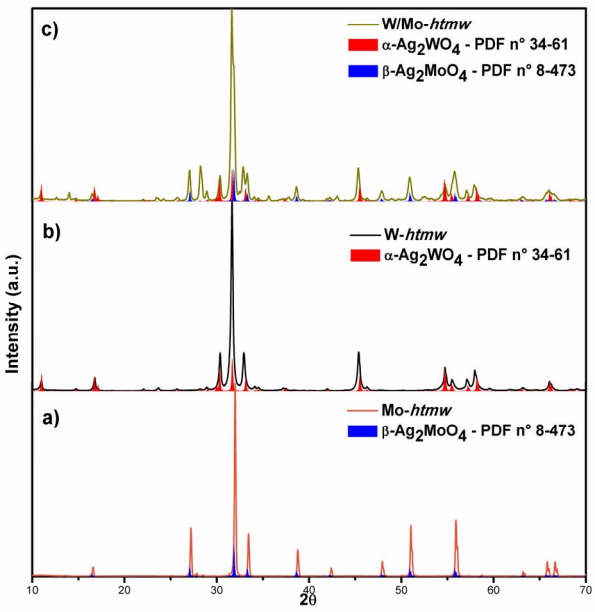

Figure 1. X-ray powder patterns of: a) β-Ag_2MoO_4 (Mo-*htmw*); b) α-Ag_2WO_4 (W-*htmw*); c) α-Ag_2WO_4/β-Ag_2MoO_4 (W/Mo-htmw)

Only some exaltation of the intensity of the 131st peak of the tungstate should be mentioned (for which any orientation effect was ruled out because its harmonic was not affected). It is worth noting that the W/Mo-*htmw* was prepared at pH 4, as experiments at pH 7 failed. This observation prompted the use of pH 4 in the second set of syntheses.

The powder XRD patterns of the samples prepared at atmospheric pressure (pH 4) without the assistance of additional energy are given in Figure 2. Mo-*70* appears again as pure spinel β-Ag_2MoO_4, although this phase is commonly obtained in neutral or alkaline media, as mentioned above. In contrast, the obtained silver tungstate is a mixture of the two orthorhombic α- and hexagonal β- allotropes, where the latter is strongly dominant. This result was actually unexpected, as the stable phase is the α- phase and was systematically obtained by various methods [17,22,40,44-46], including the "coprecipitation" approach proposed by Calvacante [15]. Indeed, the β-phase was previously obtained only by precipitation in ice water at pH 9 [16], or as metastable hollow spheres, using PMMA cross-linked micelles as templates [18]. The choice of temperature and pH appears crucial, as any change leads to the α-allotrope, as seen in the literature data. As expected, the decorated Mo/W-*70* exhibited superimposition of the patterns of the two precursors. In contrast, in the case of W/Mo-*70* (not shown) it appeared that the β-Ag_2WO_4 was almost fully transformed in the stable α-phase, due to a longer time at 70 °C, but in addition, significant decomposition occurred, as indicated by the emergence of Ag_2O peaks; this sample was not studied further.

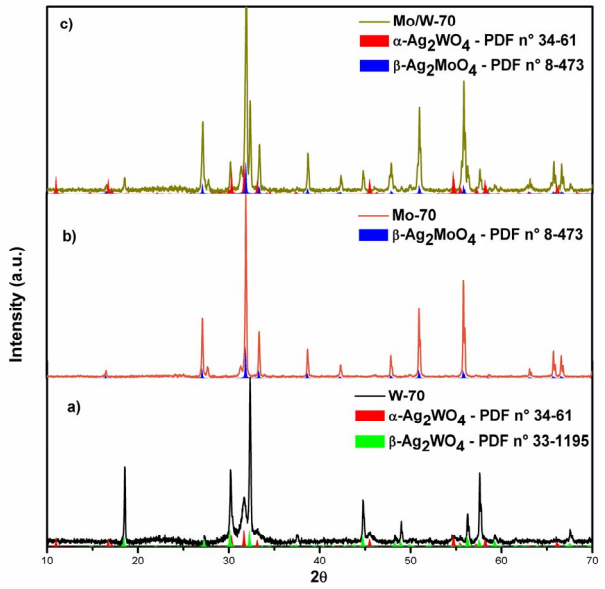

Figure 2. X-ray powder patterns of: a) β-Ag_2WO_4 (W-*70*); b) β-Ag_2MoO_4 (Mo-*70*); c) β-Ag_2MoO_4/β-Ag_2WO_4 (Mo/W-*70*)

3.2 Microstructure

The microstructure of the as-prepared and the composite compounds was revealed by FE-SEM images. Figure 3 displays the photographs of the -*htmw* samples. As can be seen, Mo-*htmw* was crystallized in the form of short nanorods with a homogeneous size (200 nm by 1 μm) (Figure 3a) and W-*htmw* appeared in the form of microsized irregular polyhedral crystals (Figure 3b). The latter were accompanied by a few microribbons that were thought to be the same α-Ag_2WO_4 phase on the basis of XRD data. W/Mo-*htmw* images showed mainly micrometric balls exhibiting very compact coverage by platelets, about 200 nm wide (Figure 3, c and d). In addition, some ribbons looked similar to those present in the starting W-*htmw*, but they were not isolated separately and appeared to have been partly dissolved, probably by an Ostwald ripening mechanism.

The microstructures of the -*70* samples are shown in Figure 4. In contrast to Mo-*htmw*, the Mo-*70* sample showed crystals of two different types Figure 4a): nanowires several dozen μm long and 100-200 nm in diameter, which closely resembled the monoclinic $Ag_2Mo_2O_7$ fibres often obtained in hydrothermal experiments carried out at pH 4 [32,40,43].

However, from the XRD data, the formation of this silver dimolybdate was ruled out. These nanowires coexisted with well-shaped cubic or cuboctahedral microcrystals, almost monodisperse in size (about 3 μm) and contrasting with the irregular nanoparticles usually observed for hydrothermally grown (at a pH of about 7-8) Ag_2MoO_4 samples [32,39-40,43]. Although exhibiting very different morphologies, these two types of crystals clearly belonged to the same β-Ag_2MoO_4 phase. as proven by the XRD data.

Concerning W-*70*, FE-SEM micrographs also showed two types of crystals, i.e., nanowires and polyhedral microcrystals (Figure 4b). In this case, because XRD data clearly showed that the sample contained the two phases α- and β-Ag_2WO_4, it would be reasonable to attribute the quasispherical crystals to the minor phase α- of the orthorhombic structure and the nanowires to the hexagonal β-phase.

On the FE-SEM micrograph of Mo/W-*70*, one can observe a number of spherical features, including the sea urchin-like surface, which is made of interpenetrated nanowires forming a continuous, felted coating (Figure 4, c and d). These microspheres appeared to be on average slightly larger than the crystals previously attributed to Mo-*70*, suggesting that W-*70* nanowires were grown on the latter crystals. This coverage was not homogeneous for all Mo-*70* cuboctahedral microcrystals, because some of them had compact coverage, while others were only partly covered. In addition, some free-standing nanowires were observed;

however, it could not be determined whether they consisted of unmodified remaining Mo-*70*, or free W-*70* nanowires newly formed in solution during the final step of the synthesis.

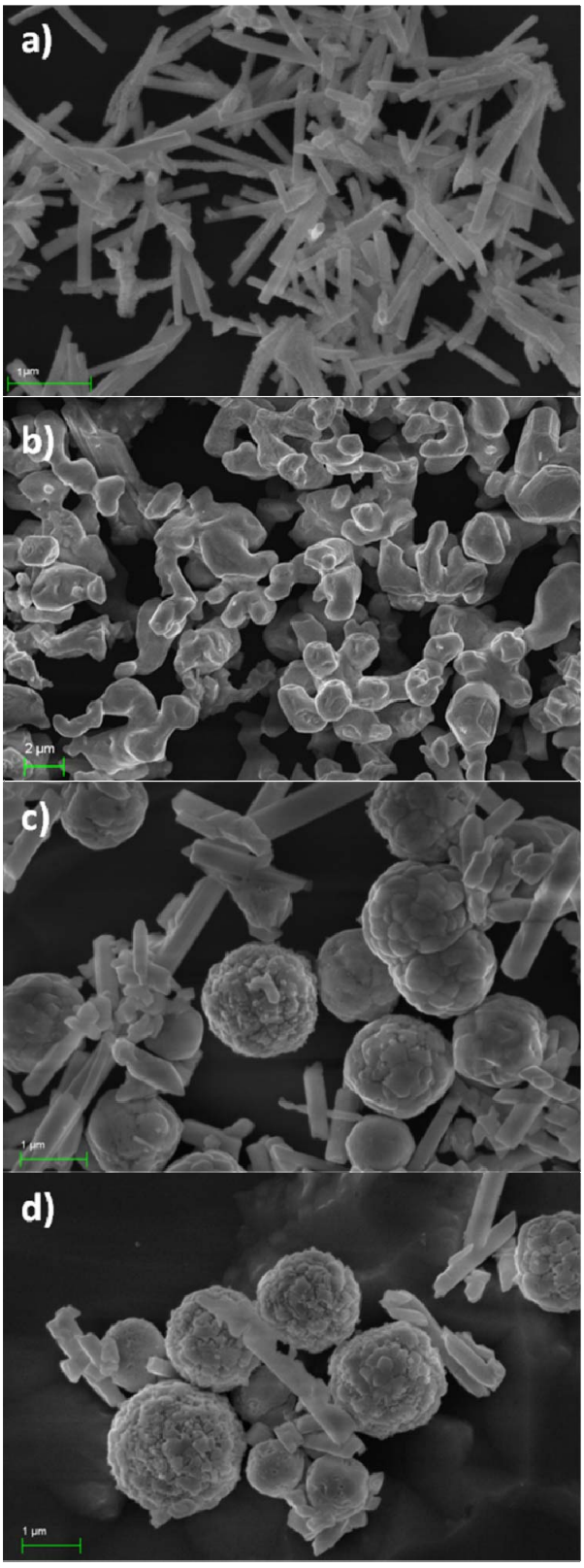

Figure 3. SEM image of: a) β-Ag_2MoO_4 (Mo-*htmw*); b) α-Ag_2WO_4 (W-*htmw*); c) and d) decorated nanoparticles α-Ag_2WO_4/β-Ag_2MoO_4 (W/Mo-*htmw*)

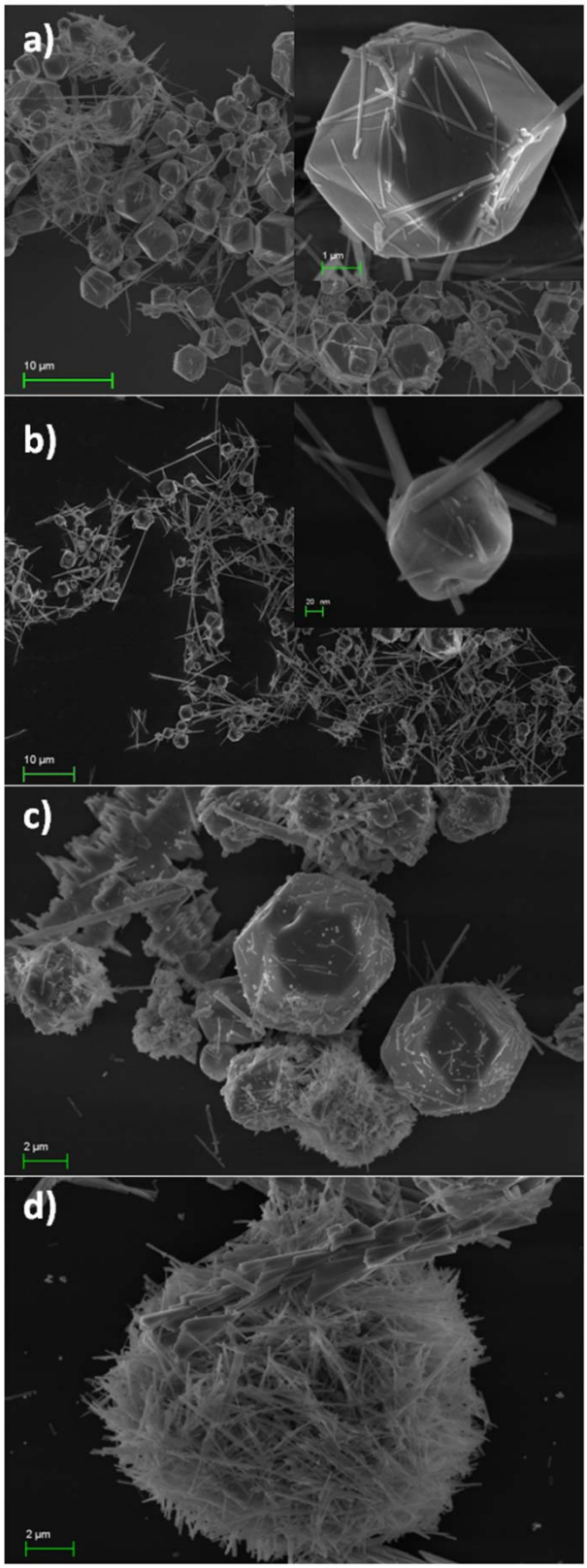

Figure 4. SEM image of: a) β-Ag_2MoO_4 (Mo-*70*); b) α- and β-Ag_2WO_4 (W-*70*); c) and d) decorated nanoparticles β-Ag_2MoO_4/β-Ag_2WO_4 (Mo/W-*70*)

3.3 Optical absorption

The UV-visible diffuse reflectance spectra of Mo-*70*, W-*70* and composites Mo/W-*70* and W/Mo-*htmw* were recorded and the optical band-gap energy (E_g) was calculated using the method of Kubelka and Munk-Aussig [48]. As seen in Figure 5, for these four examples, a straight line was found when plotting $[F(R)h\nu]^2$, meaning an exponent $n = ½$ in the classical formula $\alpha h\nu = C(h\nu - E_g)^n$, which is the signature of a direct band-gap. There are only limited data in the literature concerning the band-gaps of molybdates and -tungstates with monovalent counter cations. Z.Q. Li reported an indirect gap of 3.37 eV for a β-Ag_2MoO_4 sample prepared at 180 °C by microwave assisted hydrothermal synthesis [49], while for $Ag_2Mo_2O_7$, quite different values of 2.94 [50] and 2.65 eV (indirect) [51] were reported. Concerning the tungstates, Cavalcante et al. measured α-Ag_2WO_4 values between 3.19 and 3.23 (direct gap) [15], depending on the method of preparation, which were close to an independent estimation of 3.10 [52]. A theoretical calculation afforded a slightly larger value of 3.55 eV [17]. However, the compounds reported here belong (at least, primarily) to the β-Ag_2WO_4 allotrope, a definitively different structure.

3.4 Photoluminescence

The photoluminescence of $AMoO_4$ and AWO_4 compounds has been largely documented, especially in examples where A is a divalent cation, such as Pb or an alkaline earth [22-24,40,53-58]. As a general rule, multiphonon processes occur i.e., a system in which relaxation occurs by several paths, involving the participation of numerous states within the band gap of the material, leading to several emission bands. It is well known that the high energy component of the PL emission is an emission mainly attributed to charge-transfer transitions within the $(MO_4)^{2-}$ tetrahedral groups [PLg,h] or the WO_6 octahedra [15]. There is consensus about attributing the lowest energy emission bands to the creation of additional deep electronic levels in the forbidden band gap, relative to defects that can be either geometrical distortions of metal oxygen polyhedra and/or oxygen vacancies [15,23,40,55-58]. This model was clearly confirmed by first-principle calculations [55].

The PL spectra of Mo-*htmw*, W-*htmw* and W/Mo-*htmw* are shown in Figure 6. The three compounds exhibited a weak emission around 450 nm, obviously related to charge transfer transition within regular MoO_4 tetrahedra and WO_6 octahedra, respectively, as mentioned above. The PL spectrum of W/Mo-*htmw* presented a strong emission around 650 nm, while the two other compounds showed no significant emission in this wavelength range. The enhancement of the PL spectrum for the decorated sample can be explained by the presence of the Ag_2MoO_4

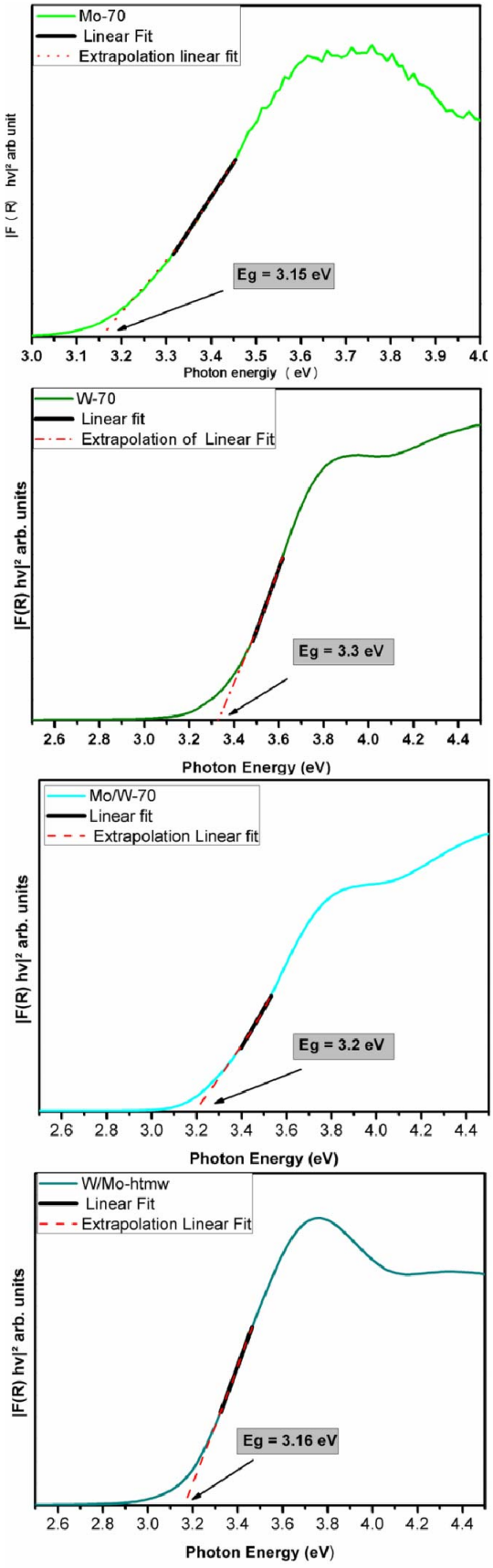

Figure 5. UV-vis spectra of β-Ag_2MoO_4 (Mo-*70*), β-Ag_2WO_4 (W-*70*), β-Ag_2MoO_4/β-Ag_2WO_4 (Mo/W-*70*) and α-Ag_2WO_4/β-Ag_2MoO_4 (W/Mo-*htmw*)

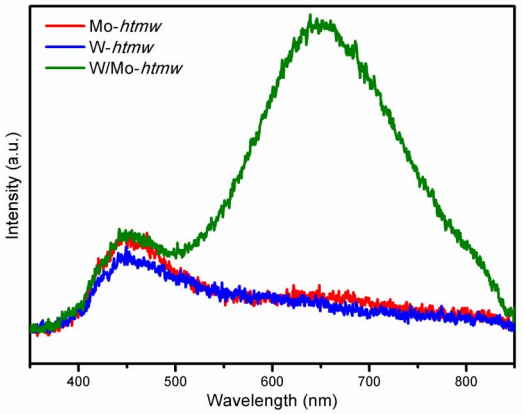

Figure 6. PL emission spectra of β-Ag_2MoO_4 (Mo-*htmw*), β-Ag_2MoO_4 (Mo-*htmw*) and α-Ag_2WO_4/β-Ag_2MoO_4 (W/Mo-*htmw*)

shell covering the surface of α-Ag_2WO_4 core, forming some structural defects at the interface and favouring the enhancement of the PL emission. Indeed, β-Ag_2MoO_4 and α-Ag_2WO_4 were built from MoO_4 tetrahedra and WO_6 octahedra, respectively; consequently, a structural distortion at the surface/interface region between these two compounds cannot be ruled out.

The samples synthesized at 70 °C without microwave assistance (Figure 7) behaved very differently from those synthesized on microwave: Mo-*70* exhibited a strong PL peak around 450 nm, originating from the charge transfer in levels very close to valence and conduction bands, and only a weak contribution near 650 nm, reflecting an ordered structure. This is in contrast to W-*70*, which is essentially a metastable phase (the β- allotrope, as shown by XRD). In the decorated Mo/W-*70*, there was also an enhancement of the long wavelength contribution, although less pronounced than in W/Mo-*htmw*. Although the actual structure of β-Ag_2WO_4 is still unknown, there is some reason to speculate that it is built from $(WO_4)^{2-}$ tetrahedra [PLk]. As a result, at the interface, the polyhedra should be less distorted. Another finding was the decrease of the intensity of the short wavelength PL peak of the molybdate core: this is indicative of good coverage by the tungstate shell.

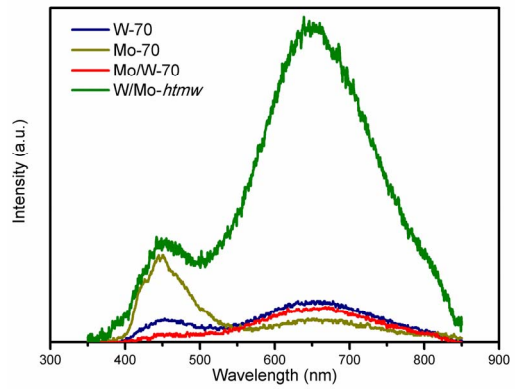

Figure 7. PL emission spectra of β-Ag_2MoO_4 (Mo-*70*); b) β-Ag_2WO_4 (W-*70*), β-Ag_2MoO_4/β-Ag_2WO4 (Mo/W-*70*) and α-Ag_2WO_4/β-Ag_2MoO_4 (W/Mo-*htmw*) for scaling

4. Conclusions

Metal molybdates and tungstates are a family of multicomponent metal oxide compounds that have been extensively studied by the scientific community as multifunctional materials, due to their interesting structures, intriguing physical-chemical properties and their diverse and prominent applications. In this study, we grew nanoparticles of Ag_2MoO_4 and Ag_2WO_4 using two complementary techniques: the MAH synthesis at 140 °C and pH 7, and a simple, co-precipitation at pH 4. The two approaches afforded the cubic β-Ag_2MoO_4; for the silver tungstate, however, the outcome was a very different result. The stable orthorhombic α-Ag_2WO_4 (i.e., $Ag_8W_4O_{16}$ built from tetrameric species of four edge-sharing distorted WO_6 octahedra) was obtained, as usual, when using MAH synthesis. In contrast, the co-precipitation at pH 4 gave, at least as the primary phase, the metastable β-Ag_2WO_4, first reported more than thirty years ago and described as a hexagonal allotrope of silver tungstate. However, this compound was never characterized in more detail and its structure remains unknown. Meanwhile, even though we failed to find any isostructural compound in the literature, it can be speculated that β-Ag_2WO_4 derives more or less from the δ-Na_2MoO_4 type [59]. If this is the case, it will be constructed, similarly to the spinel-type γ-Ag_2WO_4 allotrope, from isolated WO_4 tetrahedra. Work is currently in progress to verify this hypothesis. Nevertheless, we were able to obtain a value for its optical gap (3.3 eV) for the first time.

In a second step, these different samples were used as a basis with which to synthesize silver tungstate/molybdate (and vice-versa) composites. A strong enhancement of the low-energy photofluorescence band was evidenced in the example of α-Ag_2WO_4/β-Ag_2MoO_4. Middle-range disorder, induced by distortions of the polyhedral network and/or oxygen vacancies, was successfully invoked to explain photo-luminescence in this domain, as both created deep levels in the forbidden band. In the present case, we assumed that the pertinent defects were local, being created at the interface between the two compounds, where the MO_6 octahedra and the MO_4 tetrahedra interacted. In the reverse example of β-Ag_2MoO_4/β-Ag_2WO_4, these specific defects were absent, as both structures would contain MO_4 tetrahedra: indeed, this sample exhibited only a small enhancement of the low-energy PL band, which could be related to the more usual approach taken here [58]. Theoretical calculations are in progress to gain further insight about this possible mechanism.

It is important to know that the β-Ag_2MoO_4/α-Ag_2WO_4 and α-Ag_2WO_4/ β-Ag_2MoO_4 particles can influence the overall performance of photoluminescence. Interface effects induced by defects where the MO_6 octahedra and

the MO_4 tetrahedra interacted were local. The examples discussed in the present study provide a convenient tool for separating the two effects (surface and interface). The interface effect increased photoluminescence due to the interaction of the MO_6 and MO_4 clusters. These observations open up new opportunities for introducing both of these paradigms and synergistically enhance photoluminescence and surface-interface defects.

5. Acknowledgements

The authors are thankful for the financial support of the following Brazilian research financing institutions: CAPES, CNPq and FAPESP CEPID - CDMF 2013/07296-2, FAPESP INCTMN 2008/57872-1, CNPq INCTMN 573636/2008-7, Y. V. B. S. and would like to acknowledgment research support foundation of the state of São Paulo for the post-doctoral process n°: 2012/22823-6.

6. References

[1] Sundaram R, Nagaraja K S (2004) Electrical and humidity sensing properties of lead (II) tungstate-tungsten (VI) oxide and zinc (II) tungstate-tungsten (VI) oxide composites. Mate Res Bull 39: 581-590.

[2] Song S, Zhang Y, Xing Y, Wang C, Feng J, Shi W, Zheng G, Zhang H (2008) Rectangular AgIn (WO4) 2 Nanotubes: A Promising Photoelectric Material. Adv Funct Mater 18: 2328-2334.

[3] Rauh R D, Wang F, Reynolds J R, Meeker D L (2001) High coloration efficiency electrochromics and their application to multi-color devices. Electrochim Acta 46: 2023-2029.

[4] Cerný P, Jelínková H, Zverev P G, Basiev T T (2004) Solid state lasers with Raman frequency conversion. Prog quant electron 28: 113-143.

[5] Oi T, Takagi K, Fukazawa T (1980) Scintillation study of ZnWO4 single crystals. Appl. Phys. Lett. 36: 278-279.

[6] Benoît G, Véronique J, Arnaud A, Alain G (2011) Luminescence properties of tungstates and molybdates phosphors: Illustration on ALn(MO4)2 compounds (A = alikaline cation, Ln = lanthanides, M = W, Mo). Solid state sci. 13: 460-467.

[7] Faure N, Borel C, Couchaud M, Basset G, Templier R, Wyon C (1996) Optical properties and laser performance of neodymium doped scheelites CaWO4 and NaGd(WO4)2. Appl. Phys. B 63: 593-598.

[8] Bradler M, Baum P, Riedle E (2009) Femtosecond continuum generation in bulk laser host materials with sub-μJ pump pulses. Appl. Phys. B 97: 561-574.

[9] Pang H, Zhang C, Shi D, Chen Y (2008) Synthesis of a Purely Inorganic Three-Dimensional Porous Framework Based on Polyoxometalates and 4d−4f Heterometals. Cryst. Growth Des. 8: 4476-4480.

[10] Xue C M, Li S X, Zhang L, Sha J Q, Zheng T Y, Zhang Q N, Li L (2013) Hydrothermal Synthesis, Characterization and Electrocatalytic/Photocatalytic Activities of New Polyoxometalate Based Hybrid Compound. J. Inorg. Organomet. Polym. 23: 1468-1476.

[11] Qian Ping Wang X X G, Wei Hua Wu, Shu Xian Liu (2011) Preparation of Fine Ag2WO4 Antibacterial Powders and Its Application in the Sanitary Ceramics. Adv. Mater. Res. 284: 1321-1325.

[12] Wang P, Huang B, Qin X, Zhang X, Dai Y, Whangbo M H (2009) Ag/AgBr/WO3·H2O: Visible-Light Photocatalyst for Bacteria Destruction. Inorg. Chem. 48: 10697-10702.

[13] Pan L, Li L, Chen Y (2013) Synthesis and electrocatalytic properties of microsized Ag2WO4 and nanoscaled MWO4 (M=Co, Mn). J. Sol-Gel Sci. Technol. 66: 330-336.

[14] Stone D, Liu J, Singh D P, Muratore C, Voevodin A A, Mishra S, Rebholz C, Ge Q, Aouadi S M (2010) Layered atomic structures of double oxides for low shear strength at high temperatures. Scripta Mater. 62: 735-738.

[15] Cavalcante L S, Almeida M A P, Avansi W, Tranquilin R L, Longo E, Batista N C, Mastelaro V R, Li M S (2012) Cluster Coordination and Photoluminescence Properties of α-Ag2WO4 Microcrystals. Inorg. Chem. 51: 10675-10687.

[16] van den Berg A J, Juffermans C A H (1982) The polymorphism of silver tungstate Ag2WO4. J. Appl. Crystallogr. 15: 114-116.

[17] Longo E, Cavalcante L S, Volanti D P, Gouveia A F, Longo V M, Varela J A, Orlandi M O, Andres J (2013) Direct in situ observation of the electron-driven synthesis of Ag filaments on alpha-Ag2WO4 crystals. Scientific Reports 3: 1676.

[18] Xuefei W, Can F, Ping W, Huogen Y, Jiaguo Y (2013) Hierarchically porous metastable β-Ag 2 WO 4 hollow nanospheres: controlled synthesis and high photocatalytic activity. Nanotechnology 24: 165602.

[19] Longo E, Voanti D P, Longo V M, Gracia L, Nogueira I C, Almeida M A P, Pinheiro A N, Ferrer M M, Cavalcante L S, Andres J (2014) Toward an Understanding of the Growth of Ag Filaments on alpha-Ag2WO4 and Their Photoluminescent Properties: A Combined Experimental and Theoretical Study. J. Phys. Chem. C 118: 1229-1239.

[20] Longo V M, De Foggi C C, Ferrer M M, Gouveia A F, André R S, Avansi W, Vergani C E, Machado A L, Andrés J, Cavalcante L S, Hernandes A C, Longo E (2014) Potentiated Electron Transference in α-Ag2WO4 Microcrystals with Ag Nanofilaments as Microbial Agent. J. Phys. Chem. A. DOI: 10.1021/jp410564p

[21] da Silva L F, Catto A C, Avansi W, Cavalcante L S, Andres J, Aguir K, Mastelaro V R, Longo E (2014) A novel ozone gas sensor based on one-dimensional (1D) [small alpha]-Ag2WO4 nanostructures. Nanoscale 6: 4058-4062.

[22] Amberg M, Günter J R, Schmalle H, Blasse G (1988) Preparation, crystal structure, and luminescence of magnesium molybdate and tungstate monohydrates, MgMoO4 H2O and MgWO4 H2O. J. Solid State Chem. 77: 162-169.

[23] Marques A, Motta F, Leite E, Pizani P, Varela J, Longo E, De Melo D (2008) Evolution of photoluminescence as a function of the structural order or disorder in CaMoO4 nanopowders. J. Appl. Phys. 104: 043505.

[24] Ryu J H, Yoon J W, Lim C S, Oh W C, Shim K B (2005) Microwave-assisted synthesis of CaMoO4 nano-powders by a citrate complex method and its photoluminescence property. J. Alloy Compd. 390: 245-249.

[25] Arora A K, Nithya R, Misra S, Yagi T (2012) Behavior of silver molybdate at high-pressure. J. Solid State Chem. 196: 391-397.

[26] Wyckoff R W G (1922) The crystal structure of silver molybdate. American Chemical Society 44: 1994-1998.

[27] Donohue J, Shand W (1947) The Determination of the Interatomic Distances in Silver Molybdate, Ag2MoO4. American Chemical Society 69: 222-223.

[28] Gulbiński W, Suszko T (2006) Thin films of MoO3-Ag2 O binary oxides – the high temperature lubricants. Wear 261: 867-873.

[29] Liu E Y, Wang W Z, Gao Y M, Jia J H (2012) Tribological Properties of Adaptive Ni-Based Composites with Addition of Lubricious Ag2MoO4 at Elevated Temperatures. Tribol. Lett. 47: 21-30.

[30] Sanson A, Rocca F, Armellini C, Ahmed S, Grisenti R (2008) Local study on the MoO4 units in AgI-doped silver molybdate glasses. J. Non-Cryst. Solids 354: 94-97.

[31] Fodjo E K, Li D W, Marius N P, Albert T, Long Y T (2013) Low temperature synthesis and SERS application of silver molybdenum oxides. J. Mater. Chem. A 1: 2558-2566.

[32] Singh D P, Sirota B, Talpatra S, Kohli P, Rebholz C, Aouadi S M (2012) Broom-like and flower-like heterostructures of silver molybdate through pH controlled self-assembly. J. Nanopart. Res. 14: 1-11.

[33] Bhattacharya S, Ghosh A (2007) Silver molybdate nanoparticles, nanowires, and nanorods embedded in glass nanocomposites. Phys. Rev. B 75: 092103.

[34] Cheng L, Shao Q, Shao M, Wei X, Wu Z (2009) Photoswitches of One-Dimensional Ag2MO4 (M = Cr, Mo, and W). J. Phys. Chem. C 113: 1764-1768.

[35] Li Z, Chen X, Xue Z L (2013) Microwave-assisted hydrothermal synthesis of cube-like Ag-Ag2MoO4 with visible-light photocatalytic activity. Sci. China Chem. 56: 443-450.

[36] Nagaraju G, Chandrappa G T, Livage J (2008) Synthesis and characterization of silver molybdate nanowires, nanorods and multipods. Bull. Mater. Sci. 31: 367-371.

[37] Bao Z Y, Lei D Y, Dai J, Wu Y (2013) In situ and room-temperature synthesis of ultra-long Ag nanoparticles-decorated Ag molybdate nanowires as high-sensitivity SERS substrates. Appl. Surf. Sci. 287: 404-410.

[38] Beltrán A, Gracia L, Longo E, Andrés J (2014) First-Principles Study of Pressure-Induced Phase Transitions and Electronic Properties of Ag2MoO4. J. Phys. Chem. C 118: 3724-3732.

[39] Wang G, Hao C, Zhang Y (2008) Microwave-assisted synthesis and characterization of luminescent lead tungstate microcrystals. Mater. Lett. 62: 3163-3166.

[40] Siqueira K F, Moreira R, Valadares M, Dias A (2010) Microwave-hydrothermal preparation of alkaline-earth-metal tungstates. J. Mater. Sci. 45: 6083-6093.

[41] Raubach C W, de Santana Y V B, Ferrer M M, Longo V M, Varela J A, Avansi Jr W, Buzolin P G C, Sambrano J R, Longo E (2012) Structural and optical approach of CdS/ZnS core-shell system. Chem. Phys. Lett. 536: 96-99.

[42] Raubach C W, Krolow M Z, Mesko M F, Cava S, Moreira M L, Longo E, Carreno N L V (2012) Interfacial photoluminescence emission properties of core/shell Al2O3/ZrO2. Cryst. Eng. Comm. 14: 393-396.

[43] Lin J, Wang Q, Zheng Y, Zhang Y (2013) Supersonic microwave co-assistance (SMC) efficient synthesis of red luminescent Eu3+ activated silver molybdates and their phase-dependent evolution processes. Cryst. Eng. Comm. 15: 5668-5672.

[44] George T, Joseph S, Mathew S (2005) Synthesis and characterization of nanophased silver tungstate. J. Phys. 65: 793-799.

[45] Hu B, Wu L H, Liu S J, Yao H B, Shi H Y, Li G P, Yu S H (2010) Microwave-assisted synthesis of silver indium tungsten oxide mesocrystals and their selective photocatalytic properties. Chem. Commun. 46: 2277-2279.

[46] Wang X, Li S, Yu H, Yu J (2011) In situ anion-exchange synthesis and photocatalytic activity of Ag8W4O16/AgCl-nanoparticle core-shell nanorods. J. Mol. Catal. A-Chem. 334: 7.

[47] Cui X, Yu S H, Li L, Biao L, Li H, Mo M, Liu X M (2004) Selective Synthesis and Characterization of Single-Crystal Silver Molybdate/Tungstate Nanowires by a Hydrothermal Process. Chem. Eur. J. 10: 218-223.

[48] Kubelka P, Munk F (1931) Ein Beitrag zur Optik der Farbanstriche Zeit. Für.Tech. Physik. 12: 8.

[49] Li ZQ, Chen XT, Xue ZL (2013) Microwave-assisted hydrothermal synthesis of cube-like Ag-Ag2MoO4 with visible-light photocatalytic activity. Science China-Chemistry 56:443-450.

[50] Hashim M, Hu C, Chen Y, Zhang C, Xi Y, Xu J (2011) Synthesis, characterization, and optical properties of Ag2Mo2O7 nanowires. Phys. Status Solidi. A 208: 1937-1941.

[51] Kim D W, Cho I S, Lee S, Bae S T, Shin S S, Han G S, Jung H S, Hong K S (2010) Photophysical and Photocatalytic Properties of Ag2M2O7 (M=Mo, W). American Chemical Society 93: 3867-3872.

[52] Tang J, Ye J (2005) Correlation of crystal structures and electronic structures and photocatalytic properties of the W-containing oxides. J. Mater. Chem. 15: 4246-4251.

[53] Van Loo W (1975) Luminescence decay of lead molybdate and lead tungstate — A descriptive model. J. Lumin. 10: 5.

[54] Groenink J A, Blasse G (1980) Some new observations on the luminescence of PbMoO4 and PbWO4. J. Solid State Chem. 32: 12.

[55] Longo V M, Orhan E, Cavalcante L S, Porto S L, Espinosa J W M, Varela J A, Longo E (2007) Understanding the origin of photoluminescence in disordered Ca0.60Sr0.40WO4: An experimental and first-principles study. Chem. Phys. Lett. 334: 9.

[56] Korzhik M V, Pavlenko V B, Timoschenko T N, Katchanov V A, Singovskii A V, Annenkov A N, Ligun V A, Solskii I M, Peigneux J P (1996) Spectroscopy and Origin of Radiation Centers and Scintillation in PbWO4 Single Crystals. Phys. Status Solidi A 154: 779-788.

[57] Cavalcante L S, Sczancoski J C, Lima L F, Espinosa J W M, Pizani P S, Varela J A, Longo E (2008) Synthesis, Characterization, Anisotropic Growth and Photoluminescence of BaWO4. Cryst. Growth Des. 9: 1002-1012.

[58] Anicete-Santos M, Picon F C, Escote M T, Leite E R, Pizani P S, Varela J A, Longo E (2006) Room temperature photoluminescence in structurally disordered SrWO4. Appl. Phys. Lett. 88: 211913.

[59] Bramnik K G, Ehrenberg H (2004) Study of the Na2O-MoO3 System. Na6Mo11O36 — a New Oxide with Anatase-related Structure, and the Crystal Structures of Na2MoO4. Zeitschrift für anorganische und allgemeine Chemie 630: 1336-1341.